FUDMA Journal of Engineering and Technology
ISSN: 3092-9385
https://fjet.fudutsinma.edu.ng/index.php/fjet/
Volume 2, Issue 2, 2026, 238-258

Evaluation of Nano-Hydroxyapatite/Nano-Kaolin Composite Additives on the Physical Properties of Hot Mix Asphalt Binder

Sani MAMOUDOU[1*], Abdulmumin A. SHUAIBU[2], Aliyu USMAN[3]

[1*,2,3]Department of Civil Engineering, Ahmadu Bello University, Zaria, Nigeria

[1*]mamoudouibrahim5161@gmail.com, [2]abdulshub4u@gmail.com, [3]auzaria@abu.edu.ng

Abstract
This study evaluates the impact of a nano-hydroxyapatite (NHAp) and nano-kaolin clay (NKc) blend on the physical properties of penetration-grade asphalt binder, to enhance binder performance and durability. NHAp was synthesised from discarded animal bones, while the NKc was processed from the Kankara kaolin deposit. A response surface methodology (RSM)-based central composite design (CCD) was employed to blend NHAp and NKc and to test the physical properties of the conventional hot mix asphalt binder, including penetration, softening point, ductility, flash and fire points, and viscosity. Furthermore, RSM was used for mathematical modelling and optimisation of the desired physical properties of HMA binder. Results revealed a progressive reduction in penetration (66.3 mm to 35.3 mm) and an increase in viscosity (81 s to 122 s), indicating enhanced stiffness and resistance to deformation. The softening point increased moderately (45 °C to 48 °C, reflecting improved high-temperature stability, while flash and fire points rose sharply (292 °C to 308 °C) and (305 °C to 320 °C), respectively, signifying improved thermal safety. However, ductility decreased significantly with higher NKc content (from 110 cm down to 74 cm), underscoring a trade-off between stiffness and flexibility. Statistical analysis (ANOVA) revealed the importance of both individual and interaction effects ($p < 0.05$) of the input variables, with NKc exerting a dominant influence on most characteristics, while NHAp performed a moderating role, particularly in maintaining ductility. Optimisation with RSM revealed an optimal blend of around 0.61% NHAp and 3.42% NKc, resulting in a balanced performance with 59% of desirability, while validation testing revealed prediction errors of less than 5%.

Keywords: *Bitumen, Hot mix asphalt, Nano-Hydroxyapatite, Nano-Kaolin, Response surface methodology.*

1.0 Introduction

Bitumen, a vital component of asphalt concrete, is prone to performance issues such as ageing, deformation, and temperature susceptibility, leading to premature pavement failures such as rutting, cracking, and moisture damage. [1]. These issues significantly reduce road service life and increase maintenance costs, particularly in regions like Nigeria, where asphalt production is expensive. Studies have shown that the quality of bitumen has a significant impact on the strength, performance, and durability properties of hot mix asphalt in service. Thus, the need to improve the quality of bitumen used in the production of hot mix asphalt.

In the search for sustainable alternatives, attention has shifted toward waste-based modifiers that are both cost-effective and environmentally sustainable. Consequently, various modifiers such as polymers and waxes have been widely applied to improve binder performance, with increased viscosity, higher softening point, and improved rutting resistance[2], [3]. Nanomaterials have emerged as a promising alternative for bitumen modifications and improvement due to their small size and large surface area. Nanomaterials have unique properties and many novel qualities that make them suitable for use as an additive in asphalt pavement in comparison to other sizes like micromaterials, milli-materials, centi-materials, etc.[4]. Several studies have demonstrated that nanomaterial modification reduces penetration, increases viscosity, and enhances stiffness and rutting resistance of asphalt binders [5], [6]. For instance, the use of nanosilica, nanoclays, and nanoiron as bitumen modifiers has been reported to decrease penetration value, increase viscosity and softening point, increase complex modulus and decrease phase angle, thereby improving ageing and mechanical properties of hot mix asphalt when used [6]. Similarly, [7] investigated the performance of asphalt binders containing the polymer nanocomposite (EVA/HDPE/nano-clay) using both conventional testing (penetration, softening point, and ductility) and rheological performance tests (multiple stress creep recovery, dynamic shear rheometer, and bending beam rheometer). They discovered that, regardless of whether the asphalt binder exhibited linear or nonlinear viscoelastic behaviour, the polymer nanocomposite improved resistance to cracking and rutting. Despite the numerous advantages of nanomaterials modification, they have often introduced trade-offs; for example, nano-clay has been reported to reduce ductility and negatively affect low-temperature performance at higher dosages [8]. Consequently, recent research suggests combining different nanomaterials to produce a synergistic effect capable of overcoming individual limitations [5]. This study evaluates the impact of a nano-hydroxyapatite

Received: 15/07/2026; Revised: 29/07/2026; Accepted: 09/08/2026; Published: 17/08/2026

(NHAp) and nano-kaolin clay (NKc) blend on the physical properties of penetration-grade asphalt binder, with the aim of enhancing binder performance and durability.

Nano-hydroxyapatite (NHAp), known to be bioactive due to its mineral composition and its structural reinforcing properties, is recognised by [9] since it can provide a possibility for synergistic enhancement when combined with other nanomaterials. However, its limited mechanical strength reduces its effectiveness as a stand-alone asphalt modifier. Consequently, there is a need to reinforce its mechanical properties and then create a stronger additive material. Unfortunately, most additives are detrimental to the biological properties of HAp. Therefore, the inclusion of kaolin due to its non-toxicity as a second modifier to reinforce HAp in the asphalt mixture attracted attention. Despite this potential, there is still limited investigation into the combined effect of NHAp and NKc on the conventional physical properties of asphalt binder. Most existing studies have focused on single nanomaterial modification, leaving a clear gap in understanding the interaction and optimisation of hybrid nanomaterial systems. Prior research has demonstrated that even small percentages of nano-clay significantly improve asphalt binder stiffness and shear modulus, indicating enhanced load-bearing capacity and performance.[5]. [10] studied the effect of NHAp in cementitious materials and reported significant improvements in tensile and flexural strengths compared to control materials. In addition, the use of waste-derived materials such as animal bones for NHAp production provides a sustainable solution by reducing environmental pollution and promoting resource utilisation. [11]. Therefore, this study evaluates the synergistic effect of nano-hydroxyapatite and nano-kaolin clay blend on the physical properties of asphalt binder. Conventional tests, including penetration, softening point, ductility, viscosity, and thermal properties, are conducted to assess performance, while Response Surface Methodology (RSM) is employed to model and optimise the modifier content. This study aims to develop a sustainable and high-performance asphalt binder through an optimised nanomaterial blend.

1.2 Research gaps

Despite prior research that focused most generally on individual nanomaterial modifiers, this work assesses the combined effect of a waste-derived nano-hydroxyapatite (NHAp) and nano-kaolin clay (NKc) composite on asphalt binder characteristics. The study also integrates the Response Surface Methodology (RSM) via Central Composite Design (CCD) to develop predictive models and determine the optimum hybrid nanomaterial dosage for improved binder performance.

2.0 Materials and Methods

2.1. Materials

The materials used for this research work are penetration-grade bitumen sourced from MotherCat Construction Company Nigeria Limited, Zaria. The non-separated biowastes (animal bones) which include an approximate percentage of caprine, galline, porcine, or other bones scavenged, were obtained from an abattoir dumping site in Zango, Zaria. The kaolin was collected from a deposit in Kankara Local Government Area of Katsina State, Nigeria.

2.2 Methods

Figure 1 below is the summarised flow chart of the methodology employed in this study.

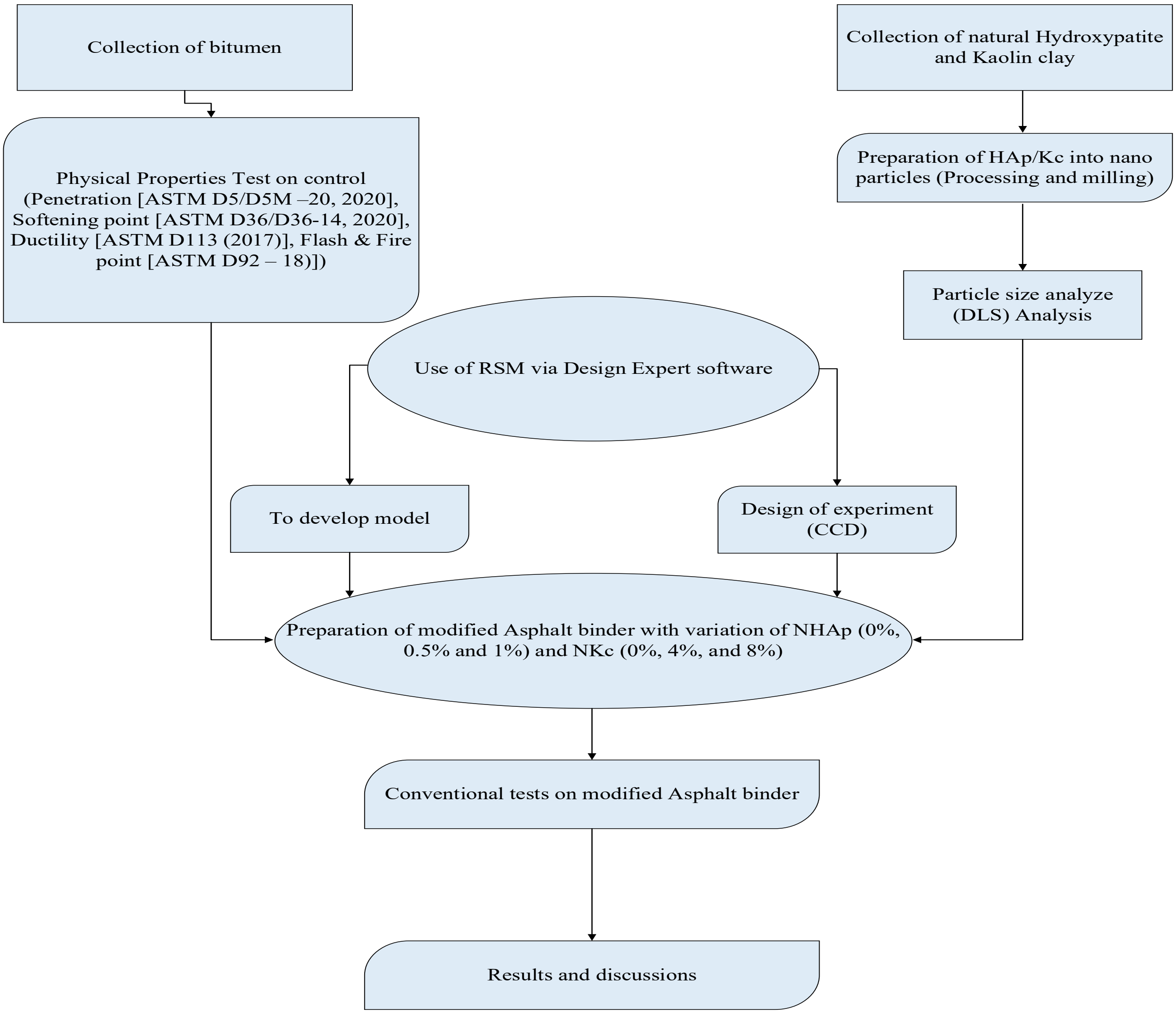

Figure 1: Flow chart for the Research methods

2.2.1 Preparation of NHAp and NKc

The animal bones were properly cleaned and washed using tap water. In order to deproteinize, the washed bone samples were boiled for 3 h and dried at 150 °C for 8 h. Then, the sample was heat-treated at temperatures of 900 °C, 1000 °C, and 1100 °C consecutively to obtain a clear white sample (hydroxyapatite). This process was carried out in the Shells laboratory in the Department of Mechanical, Amadu Bello University, Zaria. Furthermore, the sample was ball milled for 50 hours at the Department of Chemical Engineering, ABU, Zaria to obtain the nano form of hydroxyapatite. Similarly, the kaolin was ball milled to transform it into a nanoscale form.

2.2.2 Particle Size Analysis

Particle size analysis (PSA) is an important technique for determining particle size distribution. The dynamic light scattering (DLS) method was used in this case study. Also known as photon correlation spectroscopy (PCS), DLS is the most often used method for measuring nanoparticle size. The nanoscale nature of the synthesised hydroxyapatite and kaolin was later confirmed through this DLS analysis, which showed that the majority of particles fell within the nanometer range, indicating successful size reduction and synthesis of NHAp and NKc. This transformation preserved the mineral composition of hydroxyapatite and kaolin while enhancing their surface area and reactivity, making them suitable for asphalt binder modification. The test was carried out in accordance with the standard at Malvern Central Lab, Minna University.

2.2.3 Modified Bitumen Preparation

First, the bitumen was heated in an oven at 145 °C to 150 °C to make it fluid enough for mixing. Nano-hydroxyapatite (NHAp) was investigated within the low concentrations ranging from 0, 0.5 and 1% because most previous studies. [9], [12] etc. used it for medical purposes. Nano-kaolin clay (NKc) was investigated within 0, 4 and 8% in consistent with dosage ranges commonly reported from literature for nanoclay modification of asphalt binders. [13], [14], [15] etc. Following the mix design generated by RSM (CCD) via Central Composite Design

(CCD) which is employed to generate thirteen experimental combinations within these ranges, allowing evaluation of the individual, quadratic, and interaction effects of NHAp and NKc on the physical properties of the asphalt binder, the two nanomaterials were then added gradually to the 60/70 penetration grade bitumen at different percentage and mixing manually for 60 minutes to form a homogenous material. Subsequently, the physical properties of the modified bitumen were tested.

2.2.4 Response surface method (RSM)

Response surface methodology (RSM) is a combination of mathematical and statistical techniques used for the development and improvement. The Response Surface Methodology (RSM) was chosen since the study included two interacting process variables (NHAp and NKc) and various performance responses. Compared to the traditional one-factor-at-a-time approach, RSM allows for the simultaneous examination of the individual, interaction, and quadratic effects of the modifiers while significantly reducing the number of laboratory tests necessary. The Central Composite Design (CCD) was chosen because it efficiently estimates second-order polynomial models and allows numerical optimisation of numerous response variables to identify the optimal modifier combination. An optimal quadratic predictor model, shown in equation 1, was used to develop the mathematical model and obtain the optimal conditions for the responses.

$$y = \beta_o + \sum_{i=1}^{k} \beta_i X_i + \sum_{i=1}^{k} \beta_{ii} {X_i}^2 + \sum\sum \beta_{ij} X_i X_j + e \qquad (1)$$

where y is the predicted outcome; β_0 is the experiment central point fixed response value, β_j and β_{jj} are first- and second-order effects, β_{ij} is the cross-interaction effect; X_i and X_j are coded factors, while e is a model random error. Table 1 below shows the CCD mix design generated by RSM.

Table 1: Central Composite Design Mix Design

Run	A: NHAp (%)	B: NKc (%)	Response(s)
1	0.5	4	
2	0.5	4	
3	1	4	
4	0	4	
5	0.5	0	
6	0	8	
7	0.5	4	
8	0	0	
9	0.5	8	
10	0.5	4	
11	1	0	
12	0.5	4	
13	1	8	

Source: Mamoudou et al. (2026)

2.2.5 Fourier Transform Infrared (FTIR) Spectroscopy

Fourier transform infrared (FTIR) spectroscopy is a versatile and non-destructive analytical method for characterising molecular structures, monitoring chemical reactions, and quantifying analytes in a variety of materials. FTIR spectroscopy detects the absorption of infrared light by molecules experiencing vibrational transitions between quantised energy levels. When infrared radiation interacts with a sample, particular frequencies are absorbed that correspond to molecular bond vibrations such as dipole stretching, bending, and twisting. In a typical FTIR device, a broadband IR source travels via an interferometer, most typically of the Michelson design. A moving mirror generates a succession of constructive and destructive interference patterns, which form an interferogram that encodes all spectrum frequencies at the same time. A fast Fourier transform (FFT) technique converts the interferogram into an intensity-versus-wavenumber spectrum. This test was carried out in accordance with the standard at the chemistry lab, ABU Zaria, Kaduna, Nigeria.

3.0 Results and Discussions

This section presents and discusses the experimental findings on the physical properties of asphalt binder modified with various amounts of Nano-Hydroxyapatite (NHAp) and Nano-Kaolin Clay (NKc). The properties evaluated include penetration, softening point, ductility, flash/fire point and viscosity. The central composite design (CCD) was used to generate a variety of NHAp/NKc combinations, and the results were analysed to assess the individual and combined (synergistic) impacts of the nanomaterials on the 60/70 penetration grade bitumen.

3.1 Physical properties of bitumen and the physico-chemical properties of nano-kaolin and nano-hydroxyapatite

3.1.1 Physical Properties of Bitumen (Unmodified)

The physical parameters of the unmodified penetration-grade bitumen met ASTM standards, as shown in Table 2, indicating its suitability as a control binder in HMA design. [16] reported similar compliance-based validation of binder compatibility for asphalt mixture usage.

Table 2: Physical Properties test on Unmodified Bitumen compared with the Specifications

Test conducted Bitumen	ASTM Code	Result	Specification	Remark
Penetration at 25°C, 0.1mm	ASTM D5-97	66.3	60-70	OK
Softening point (°C)	ASTMD36-12	46	45–52	OK
Ductility at 25°C, cm	ASTM D113	110	Min.100	OK
Flash point (Cleveland open cup) °C	ASTM D92-02	282	Min.232	OK
Fire point (Cleveland open cup) °C	ASTM D92-02	293	Min.232	OK
Viscosity (mm^2/secs)	ASTM D4402 (2015)	81	N/A	OK

Source: Mamoudou et al. (2026)

3.1.2 Physico-Chemical Characterisation of Nano-Materials

3.1.2.1 Particle size distribution of nano-hydroxyapatite

Figure 2 illustrates the outcome of the dynamic light scattering (DLS) analysis conducted on nano-hydroxyapatite. The Figure revealed that the NHAp sample consists of a largely monodisperse population of nanoparticles, with a Z-average hydrodynamic diameter of 30.28 nm and a polydispersity index (PdI) of 0.377, indicating a moderate size distribution. The volume- and number-weighted distributions clarified that over 99 % of the sample volume consisted of nanoparticles centred around 18–25 nm. The high correlation intercept (0.842) and low cumulants-fit error (0.00158) confirm good signal quality and reliable fitting of the primary nanoparticle population. These findings suggest that the hydroxyapatite sample is primarily made up of homogeneous nanoparticles, with only a few small levels of aggregates that have no meaningful effect on the system's overall colloidal properties.

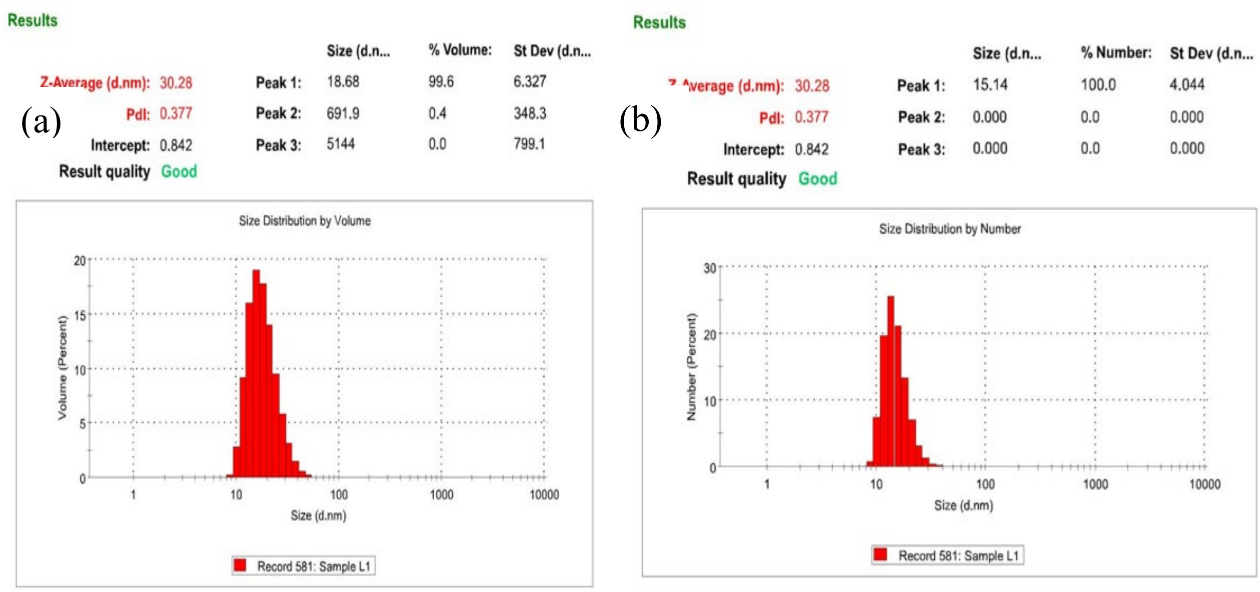

Figure 2: Graphical representation of Particle size distribution of Hydroxyapatite sample

3.1.2.2 Chemical Composition (XRD) of nano-hydroxyapatite

The XRD analysis of the synthesised hydroxyapatite, as shown in Table 3, revealed that calcium and phosphorus are the main elements in nano-hydroxyapatite, accounting for more than 80% of the total composition, indicating that the material has a calcium-phosphate structure. This finding confirms that of [9] in their study with NHAp. This composition is typical of hydroxyapatite, namely bone-derived hydroxyapatite, which is known to be non-stoichiometric due to ionic substitution. [9]. The high calcium concentration is advantageous in asphalt modification as it can improve binder-aggregate adhesion and moisture resistance. Minor elements including zirconium, barium, sodium, and magnesium are found in small amounts due to spontaneous mineral

Received: 15/07/2026; Revised: 29/07/2026; Accepted: 09/08/2026; Published: 17/08/2026

substitution during synthesis. These elements have no negative impact on the material's chemical stability and may help improve the thermal stability of the modified binder.

Table 3: Mineralogical composition (XRD) of Hydroxyapatite

Element Number	Element Symbol	Element Name	Atomic Conc.	Weight Conc.
20	Ca	Calcium	66.78	65.4
15	P	Phosphorus	22.19	16.79
40	Zr	Zirconium	6.07	13.53
56	Ba	Barium	0.48	1.61
11	Na	Sodium	1.81	1.01
12	Mg	Magnesium	1.59	0.94
13	Al	Aluminium	1.08	0.71
50	Sn	Tin	0	0
19	K	Potassium	0	0
38	Sr	Strontium	0	0
22	Ti	Titanium	0	0
26	Fe	Iron	0	0
14	Si	Silicon	0	0
16	S	Sulfur	0	0
17	Cl	Chlorine	0	0
30	Zn	Zinc	0	0
47	Ag	Silver	0	0
37	Rb	Rubidium	0	0
55	Cs	Caesium	0	0

Source: Mamoudou et al. (2026)

3.1.2.3 Particle size distribution of Kaolin sample

Figure 3 presents the outcome of the dynamic light scattering (DLS) analysis conducted on nano-kaolin. The Figure revealed a moderately polydisperse nanoparticle suspension with a Z-average hydrodynamic diameter of 27.02 nm and a polydispersity index (Pdl) of 0.584. The volume and number-weighted analysis clarified that the sample was predominantly composed of nanoparticles. The volume and number-weighted analysis clarified that the sample was overwhelmingly dominated by nanoparticles. The volume distribution indicated a principal population centred at 14.58 nm and a minor peak at 253.6 nm, while the number distribution confirmed that essentially all particles (~100% by count) were approximately 12.71 nm in size. These results indicate that the sample consists primarily of nanoscale particles with a higher polydispersity, alongside trace amounts of sub-micron aggregates. The strong intercept (0.907) and low cumulant fit error (4.93×10^{-4}) validate the reliable nature of the given size distribution.

Received: 15/07/2026; Revised: 29/07/2026; Accepted: 09/08/2026; Published: 17/08/2026

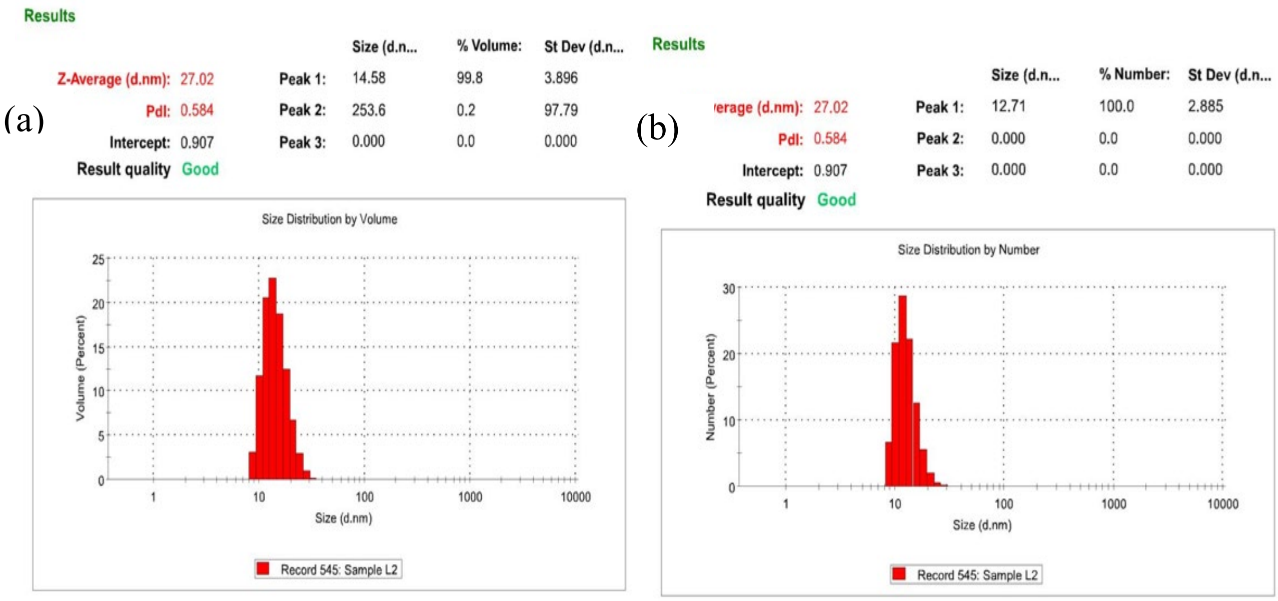

Figure 3: Graphical representation of Particle size distribution of Kaolin sample

3.1.2.4 Chemical Composition (XRD) of Kaolin clay

The XRD analysis of the kaolin clay shown in Table 4 revealed that silicon and aluminium are the most abundant constituents, accounting for over 94% of the total elemental composition of nanolaolin. This agrees with the previous submission of [13] whose study found over 90% of SiO_2 and Al_2O_3 in kaolin. This confirms the kaolinitic nature of the clay and its suitability as a reinforcing material in asphalt modification. According to [13], the kaolin clay's high SiO_2 and Al_2O_3 content improve Marshall stability and stiffness in HMA, indicating that these chemical compositions improve binder-aggregate interaction and mixture performance. Minor elements such as calcium and iron are present only in trace amounts and do not adversely affect binder performance.

Table 4: Mineralogical composition (XRF) of Kaolin sample

Element Number	Element Symbol	Element Name	Atomic Conc.	Weight Conc.
14	Si	Silicon	59.49	58.78
13	Al	Aluminium	37.96	36.03
50	Sn	Tin	0.47	1.94
16	S	Sulfur	0.93	1.05
20	Ca	Calcium	0.6	0.85
26	Fe	Iron	0.4	0.79
47	Ag	Silver	0.15	0.55
11	Na	Sodium	0	0
12	Mg	Magnesium	0	0
56	Ba	Barium	0	0
22	Ti	Titanium	0	0
40	Zr	Zirconium	0	0
30	Zn	Zinc	0	0
15	P	Phosphorus	0	0
17	Cl	Chlorine	0	0

Source: Mamoudou et al. (2026)

3.2 Effect of Modification on Conventional Binder Properties

The conventional physical properties test results presented in Table 5 show a synergetic influence of nano-hydroxyapatite (NHAp) and nano-kaolin clay (NKc) on the physical characteristics of the bitumen binder compared with the control, confirming the modifying potential of both nanomaterials within the investigated dosage range. The control binder (0% NHAp, 0% NKc) had a penetration of 66.3 mm, a softening point of 45 °C, a ductility of 110 cm, a flash point of 292 °C, and a fire point of 305 °C, indicating a relatively soft and highly workable binder. However, as NHAp and NKc content increased, penetration values decreased to as low as 35.3-

Received: 15/07/2026; Revised: 29/07/2026; Accepted: 09/08/2026; Published: 17/08/2026

36 mm at higher modifier combinations (0.5-1% NHAp with 8% NKc. Similarly, softening point values increased slightly but consistently (up to 48 °C), indicating improved high-temperature performance due to the restriction of molecular mobility within the binder matrix. These results are consistent with the findings of [17], which concluded that High-Density Polyethene (HDPE) and nano-clay (NC) modifications for asphalt binder lower penetration value while increasing softening point. However, ductility measurements revealed a susceptibility to high NKc levels, with a drop from 110 cm (control) to 74-83 cm at 8% NKc, indicating that excessive nanoclay incorporation may reduce binder flexibility while potentially increasing brittleness, a trade-off commonly observed for stiffening modifiers. This is in line with the findings of [7] and [18], which revealed reduced ductility for nano-clay-modified binders. In contrast, nanomodification considerably improved thermal safety properties: at higher NKc content, the flash point increased to 308°C and the fire point increased to 320°C, resulting in lower volatility and better ignition resistance at extreme temperatures. This result substantially confirms [15]'s argument that nanoclay improves the thermal stability and ageing resistance of bituminous binders. Furthermore, viscosity increased significantly from 81 s for the control binder to 85–122 s, with the highest value recorded at 1% NHAp and 8% NKc, indicating improved flow resistance and binder consistency.

The results reveal, in general, a clear performance balance. Modest NHAp (≈0.5-1%) combined with controlled NKc content (≤4%) improves bitumen stiffness, thermal stability, and viscosity while maintaining adequate ductility. Excessive NKc (8%) results in over-stiffening and ductility loss. This suggests that optimisation should aim for a balanced nanomaterial dosage to improve high-temperature performance while retaining binder flexibility and workability. Section 3.3.4 provides detailed explanations of the outcomes obtained here.

Table 5: Physical properties test results of Control and nanomaterial-modified bitumen

Dependent Variables		**Dependent Variables**					
A: NHAp (%)	**B: NKc (%)**	**Penetration (mm)**	**Softening Point (°C)**	**Ductility (cm)**	**Flash (°C)**	**Fire Point (°C)**	**Viscosity (mm²/secs)**
0.5	4	46.3	47.5	104	280	290	100
0.5	4	44.6	48	106.5	284	292	97
1	4	47.3	46.5	94	291	300	105
0	4	61.6	46.5	92	284	298	93
0.5	0	42.3	45.5	103	294	297	85
0	8	41	45.5	77	300	320	92
0.5	4	44.5	48	105	278	290	99
0	0	66.3	45	110	292	305	81
0.5	8	35.3	47	74	300	310	115
0.5	4	45.3	47	105	280	292	99
1	0	36	44	100	296	308	88
0.5	4	43.3	47.5	107	282	291	103
1	8	43	45.5	83	308	316	122

Source: Mamoudou et al. (2026)

3.3 Analysis of Variance (ANOVA) and model development

3.3.1 Analysis of Variance (ANOVA)

The analysis of variance (ANOVA) summary for each developed model is shown in Table 6. The model's adequacy is assessed through the F-test and lack of fit (LOF). LOF shows the data variation around the fitted model. The lack of fit for all the models developed for the physical properties of modified binder is not significant, indicating the models are adequate and fit the data excellently. All responses showed that the models' terms achieve significance at the ($P<0.05$) threshold, which translates to a 95% confidence interval. Furthermore, the model validity and adequacy were explored via the model fit summary in terms of determination coefficient R^2, Adjusted R^2, Predicted R^2, and Adequate precision is shown in Table 7. The high determination coefficient between 0.9404 and 0.9905 shows the model is capable of predicting at least 94% of the measured data. Also, the difference between the predicted and adjusted R^2 values of less than 0.2 indicates a strong correlation between the experimental and the predictive values and that the models were not overfitted. Another confirmation tool is Adequate Precision, which is a measurement of the signal-to-noise ratio. According to [19], a ratio larger than 4 indicates sufficient signal, high prediction abilities of the models, and the ability to navigate the design space. The adequate precision obtained for all the response variables is greater than 4, which implies the models are adequate.

Received: 15/07/2026; Revised: 29/07/2026; Accepted: 09/08/2026; Published: 17/08/2026

Table 6: ANOVA for the conventional properties test results

Source	Sum of Squares	df	Mean Square	F-value	p-value	
Penetration						
Model	922.44	5	184.49	145.87	< 0.0001	significant
A-NHAp	302.46	1	302.46	239.16	< 0.0001	
B-NKc	106.68	1	106.68	84.35	< 0.0001	
AB	260.82	1	260.82	206.23	< 0.0001	
A²	211.21	1	211.21	167.00	< 0.0001	
B²	131.69	1	131.69	104.13	< 0.0001	
Residual	8.85	7	1.26			
Lack of Fit	3.97	3	1.32	1.09	0.4508	not significant
Pure Error	4.88	4	1.22			
Cor Total	931.29	12				
Softening Point						
Model	17.54	5	3.51	27.84	0.0002	significant
A-NHAp	0.1667	1	0.1667	1.32	0.2879	
B-NKc	2.04	1	2.04	16.20	0.0050	
AB	0.2500	1	0.2500	1.98	0.2018	
A²	3.80	1	3.80	30.12	0.0009	
B²	5.59	1	5.59	44.34	0.0003	
Residual	0.8822	7	0.1260			
Lack of Fit	0.1822	3	0.0607	0.3470	0.7945	not significant
Pure Error	0.7000	4	0.1750			
Cor Total	18.42	12				
Ductility						
Model	1723.56	6	287.26	103.41	< 0.0001	significant
A-NHAp	0.6667	1	0.6667	0.2400	0.6416	
B-NKc	1040.17	1	1040.17	374.46	< 0.0001	
AB	64.00	1	64.00	23.04	0.0030	
A²	223.21	1	223.21	80.36	0.0001	
B²	412.86	1	412.86	148.63	< 0.0001	
A²B²	187.76	1	187.76	67.59	0.0002	
Residual	16.67	6	2.78			
Lack of Fit	10.67	2	5.33	3.56	0.1296	not significant
Pure Error	6.00	4	1.50			
Cor Total	1740.23	12				
Flash						
Model	1019.22	5	203.84	34.22	< 0.0001	significant
A-NHAp	60.17	1	60.17	10.10	0.0155	
B-NKc	112.67	1	112.67	18.91	0.0034	
AB	4.00	1	4.00	0.6714	0.4396	
A²	54.23	1	54.23	9.10	0.0195	
B²	536.01	1	536.01	89.98	< 0.0001	
Residual	41.70	7	5.96			
Lack of Fit	20.90	3	6.97	1.34	0.3797	not significant
Pure Error	20.80	4	5.20			
Cor Total	1060.92	12				
Fire point						
Model	1253.55	5	250.71	243.03	< 0.0001	significant
A-NHAp	0.1667	1	0.1667	0.1616	0.6997	
B-NKc	216.00	1	216.00	209.38	< 0.0001	
AB	12.25	1	12.25	11.87	0.0107	
A²	193.12	1	193.12	187.21	< 0.0001	
B²	456.91	1	456.91	442.91	< 0.0001	
Residual	7.22	7	1.03			

Received: 15/07/2026; Revised: 29/07/2026; Accepted: 09/08/2026; Published: 17/08/2026

Source	Sum of Squares	df	Mean Square	F-value	p-value	
Lack of Fit	3.22	3	1.07	1.07	0.4545	not significant
Pure Error	4.00	4	1.00			
Cor Total	1260.77	12				
Viscosity						
Model	1469.92	3	489.97	47.34	< 0.0001	significant
A-NHAp	400.17	1	400.17	38.66	0.0002	
B-NKc	937.50	1	937.50	90.57	< 0.0001	
AB	132.25	1	132.25	12.78	0.0060	
Residual	93.16	9	10.35			
Lack of Fit	73.96	5	14.79	3.08	0.1491	not significant
Pure Error	19.20	4	4.80			
Cor Total	1563.08	12				

Source: Mamoudou et al. (2026)

3.3.2 Diagnosing residuals to validate statistical assumptions

Table 7 provides a summary of model fit, in terms of R^2, adjusted R^2, predicted R^2, and adequate precision. The determination coefficient (R^2) is used to assess the model's degree of correlation. The R^2 values for Penetration, softening point, Ductility, Flash point, Fire point, and Viscosity are: 0.9905, 0.9521, 0.9904, 0.9607, 0.9943, and 0.9404. Correspondingly, the higher R^2 values invariably imply that the models have only 0.95%, 4.79%, 0.96%, 3.93%, 0.57% and 5.96% correlation errors. The predicted R^2 values for Penetration, softening point, Ductility, Flash point, Fire point, and Viscosity are: 0.9577, 0.8467, 0.8843, 0.8191, 0.9704, and 0.7343, respectively. The adjusted R^2 values were 0.9837, 0.9179, 0.9808, 0.9326, 0.9902, and 0.9205, respectively. This implies that all predicted R^2 values are in strong agreement with adjusted R^2 values. The regression models' quality indicator demonstrates that Predicted R^2 values are in reasonable agreement with the Adjusted R^2 values; that is, the difference in values is less than 0.2, indicating a good predictive capacity of the models. Adequate Precision, which measures the signal-to-noise ratio, can also be used as a confirmation tool. A ratio greater than 4 verifies adequate signals and indicates that the models have good predictive power, which can be used to navigate the design space. [20]. These results indicate that the predicted values obtained using regression models are extremely close to the values achieved during the experiment.

Table 7: Fit summary of the model

S/N	Response	R^2	Adjusted R^2	Predicted R^2	Adeq Precision > 4
1	Penetration	0.9905	0.9837	0.9577	42.3466
2	Softening Point	0.9521	0.9179	0.8467	14.0954
3	Ductility	0.9904	0.9808	0.8843	28.3456
4	Flash point	0.9607	0.9326	0.8191	16.1998
5	Fire point	0.9943	0.9902	0.9704	41.7488
6	Viscosity	0.9404	0.9205	0.7343	23.1605

Source: Mamoudou et al. (2026)

Equations (2-7) provide the model equations generated for all responses. For given values of each variable, the equation expressed in terms of real factors can be used to predict the outcome. The levels for each factor should be expressed in their original units.

$$\text{PENETRATION} = +45.06 - 7.10\text{A} - 4.22\text{B} + 8.08\text{AB} + 8.74A^2 - 6.91B^2 \quad (2)$$

$$\text{SOFTENING POINT} = +47.62 - 0.1667A + 0.5833B + 0.2500AB - 1.17A^2 - 1.42B^2 \quad (3)$$

$$\text{DUCTILITY} = +105.50 - 0.3333\text{A} - 13.17\text{B} + 4.00\text{AB} - 12.50A^2 - 17.00B^2 + 16.50A^2B^2 \quad (4)$$

$$\text{FLASH POINT} = +281.45 + 3.17\text{A} + 4.33\text{B} + 1.00\text{AB} + 4.43A^2 + 13.93\,B^2 \quad (5)$$

$$\text{FIRE POINT} = +290.90 + 0.1667\text{A} + 6.00\text{B} - 1.75\text{AB} + 8.36\text{A}^2 + 12.86\text{B}^2 \quad (6)$$

$$\text{VISCOSITY} = +98.38 + 8.17\text{A} + 12.50\text{B} + 5.75\text{AB} \quad (7)$$

Where A is the NHAp and B is the NKc.

Received: 15/07/2026; Revised: 29/07/2026; Accepted: 09/08/2026; Published: 17/08/2026

3.3.3 Plots of Synergetic Influence of Parameters (Predicted versus actual values)

As illustrated in Figure 4, diagnostic plots to fit statistics were developed to evaluate the appropriateness of the data.

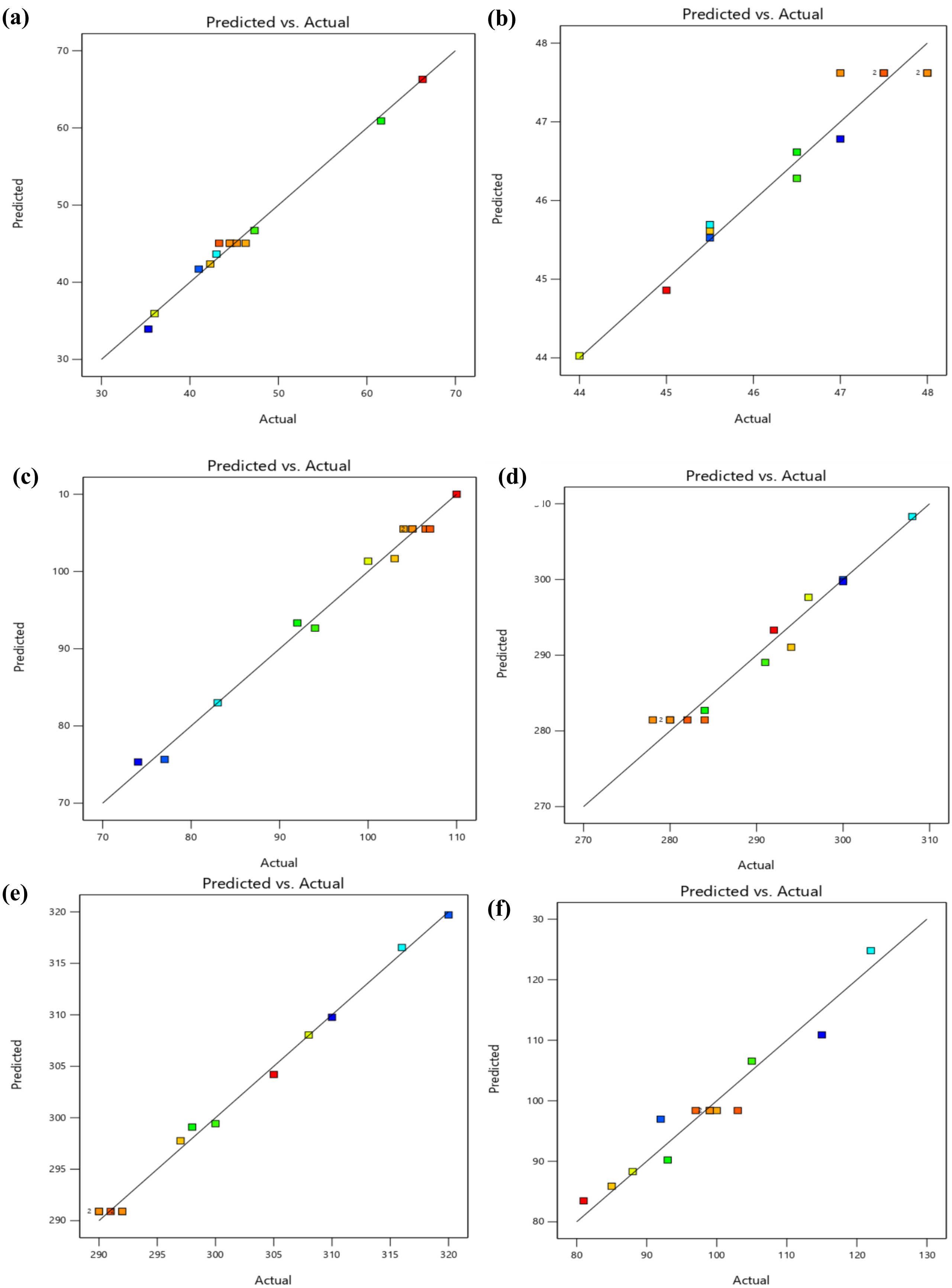

Figure 4: Plots of predicted versus actual values (a) Penetration, (b) Softening point, (c) Ductility, (d) Flash point, (e) Fire point, (f) Viscosity

Plots of predicted and actual laboratory values were also evaluated to get a better idea of how well the models performed. Almost all points were equitably distributed very close to the equality line in all of the responses, indicating that the models developed have appropriate fitting precision and have a positive correlation between predicted and actual laboratory results. Moreover, the AP values of 42.3466, 14.0954, 28.3456, 16.1998, 41.7488, and 23.1605, respectively, for Penetration, softening point, Ductility, Flash point, Fire point, and Viscosity responses are all greater than 4 $(AP > 4)$ as shown in Table 7, which is an indication that the predicted models can be used to navigate the design space defined by CCD

3.3.4 Diagnostic plots: 2D contour and 3D Surface for conventional physical properties tests on modified bitumen

3.3.4.1 Penetration

Figure 5 shows the penetration impact of NHAp and NKc modified bitumen. As can be seen from the 2D contour plots, the penetration decreases significantly with the increase of NHAp and NKc concentrations, suggesting an increased resistance to permanent deformation. The curved and elliptical contour patterns show a significant interaction between the two modifiers, which means that the penetration is governed by the combined effects of the two modifiers, not by their individual effects. This supports the highly significant interaction term (AB, F = 206.23, p < .0001). This interaction indicates that the combination of NHAp and NKc resulted in a stiffer binder than would be expected from the separate impacts of each modification, revealing the hybrid nanomaterials' synergistic behaviour. The 3D response surface indicates a non-linear decrease in penetration with increasing modifier dosage, followed by a slight flattening at higher concentrations, indicating significant quadratic terms (A^2 and B^2, p < 0.0001). The modest flattening of the response surface at increasing dosages implies that the improvement diminishes after a certain modifier content, implying that optimal rather than maximum dosages are preferable. The steeper gradient on the NHAp axis as well as the higher F value (239.16) in comparison to NKc (84.35) indicate that NHAp has a more significant impact on penetration reduction. This behaviour can be attributed to the ability of nano-hydroxyapatite to restrict the movement of bitumen molecules through its large surface area, whereas nano-kaolin enhances the binder structure, thus providing better resistance to deformation. Similarly, [6] found that nanomaterial modification lowers penetration by improving binder stiffness and resistance to permanent deformation, which is in agreement with the present results.

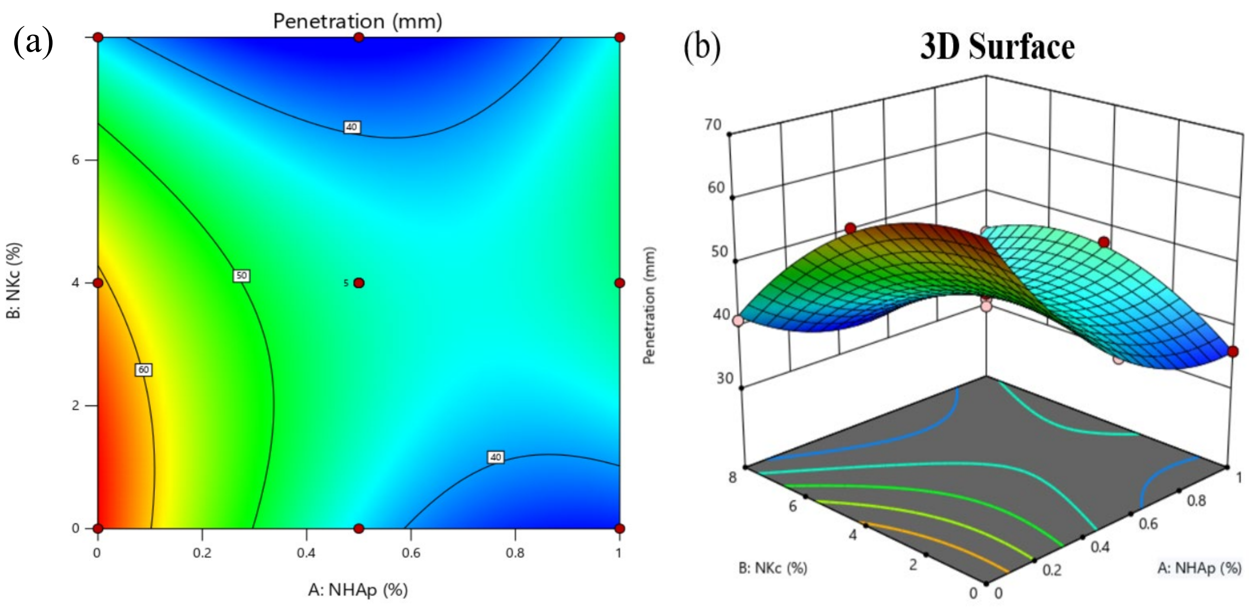

Figure 5: Diagnostic plots for Penetration (a)2D contour (b) 3D

3.3.4.2 Softening point

The softening point's 2D contour plots, Figure 6 (a), show a non-linear tendency with curved and partially closed contours, suggesting that quadratic effects predominate over purely linear behaviour. The non-significant interaction term (AB, p = 0.2018) in Table 6 is consistent with the absence of clearly elliptical shapes, indicating that NHAp and NKc primarily influence the softening point independently rather than through synergistic effects. This observation means that the increase in softening point is dominated by the specific amount of each modification (especially NKc), not a significant synergistic effect between the two nanomaterials. Similarly, the 3D response surface plots in Figure 6 (b) reveal a smoothly curved surface with a peak softening point at intermediate modifier contents, visually verifying the regression model and the importance of the quadratic terms. The curvature of the response surface indicates that increasing the modifier content beyond the optimum point

Received: 15/07/2026; Revised: 29/07/2026; Accepted: 09/08/2026; Published: 17/08/2026

does not produce a proportional increase in the softening point, highlighting the importance of dosage optimisation. From an engineering standpoint, the increased softening point achieved through controlled addition of NHAp and NKc indicates improved high-temperature performance and rutting resistance in service conditions. The enhancement may be due to the nanoparticles' ability to improve the binder matrix and restrict the movement of bitumen molecules at elevated temperature, thereby retarding the softening phenomenon. This increase in softening point with nanoparticles on asphalt binder is in agreement with [7], who reported that 2% of Polypropylene-nanoclay (EHN) could increase the rutting resistance of the asphalt binder from standard traffic level to extreme traffic level (i.e. 58S to 58E). Therefore, they concluded that the proposed polymer nanocomposite may be considered in road construction in regions that encounter high temperature changes during a day or a year.

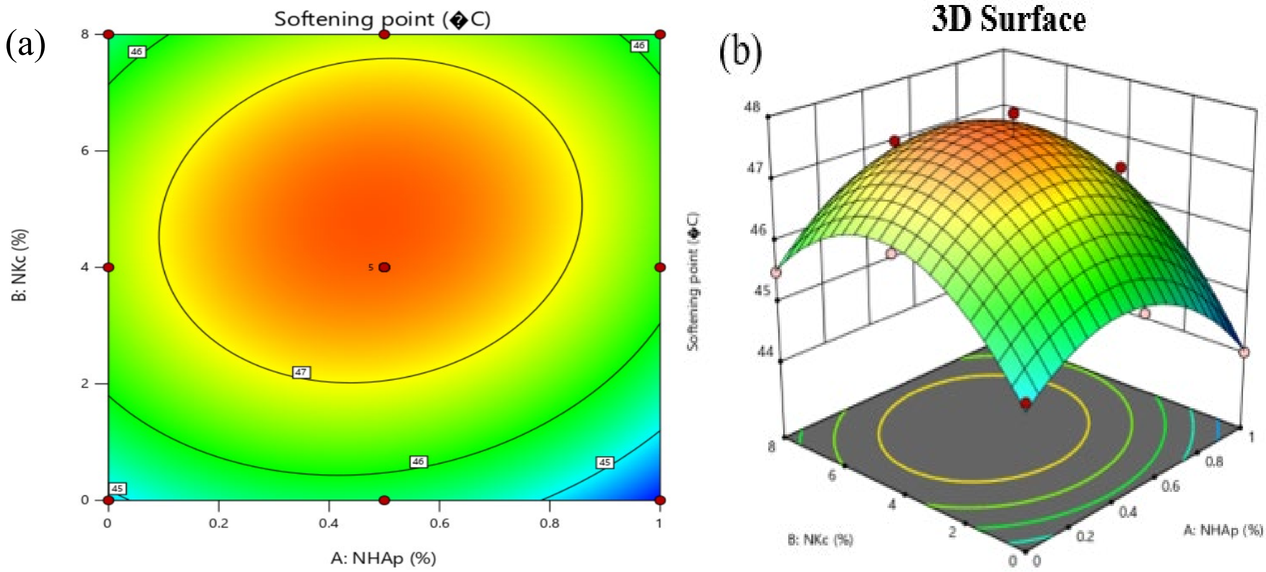

Figure 6: Diagnostic plots for Softening point (a)2D contour (b) 3D

3.3.4.3 Ductility

The contour plot (Figure 7 (a)) shows closely clustered nearly vertical contour lines with a rapid drop from high (≈100-110 cm) to low (≈70-80 cm) values, which signifies a decrease in ductility with increasing concentration of NKc. This confirms that NKc is the primary cause of ductility loss. The strong influence of NKc suggests that the stiffening effect of nanoclay becomes more dominant as its dose increases, reducing the binder's ability to withstand tensile deformation before failure. Correspondingly,[3] reported a decrease in ductility with the increase of diatomite and crumb rubber concentrations. The 3D response surface plot from Figure 7(b) shows a significant NKc impact, as indicated in Table 4 ($F = 374.46$, $p < 0.0001$), and a non-significant NHAp effect, indicating a steep fall along the NKc axis. This is consistent with the ANOVA data, which show that NKc is the primary factor affecting ductility, with NHAp contributing only moderately to this response. Nevertheless, the convex form of the 3D surface and the small curvature in the contour plot support a significant positive interaction term (AB, $p = 0.0030$), indicating that NHAp plays a moderating role when combined with NKc by partially mitigating the ductility loss caused by NKc. This interaction reveals that, whereas NHAp has no significant effect on ductility alone, its presence enhances the overall balance of stiffness and flexibility when employed in combination with NKc. From these findings, it can be concluded that while NKc shows good stiffening agent properties, excessive use reduces flexibility, and the addition of NHAp is required to achieve balanced stiffness-ductility performance through synergistic binary blending.

Received: 15/07/2026; Revised: 29/07/2026; Accepted: 09/08/2026; Published: 17/08/2026

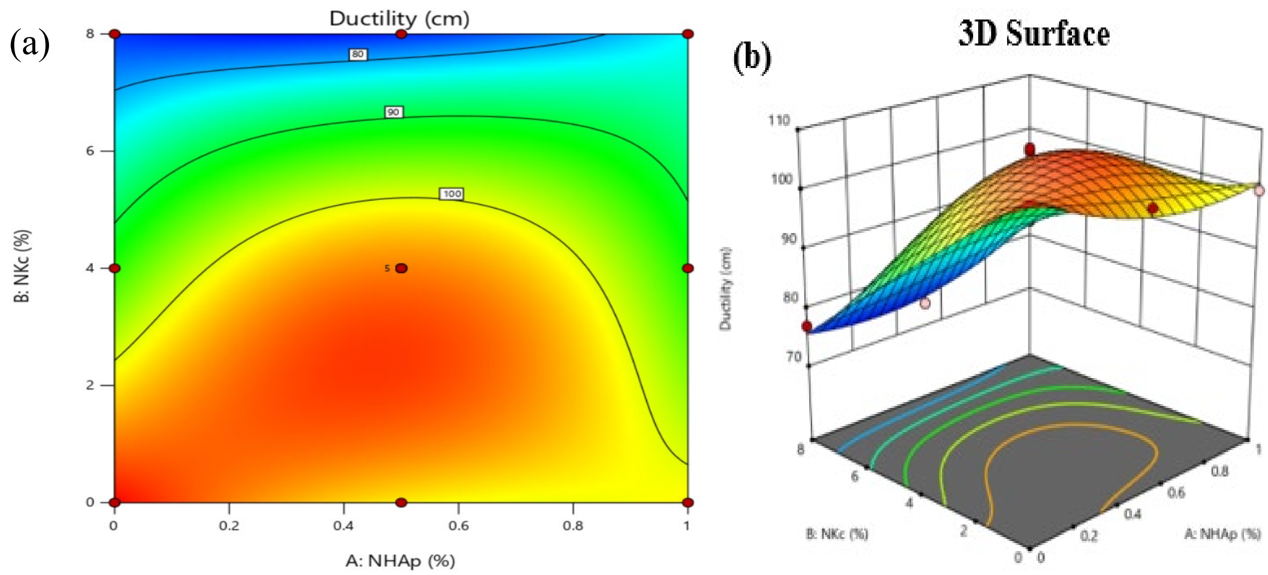

Figure 7: Diagnostic plots for Ductility (a)2D contour (b) 3D

3.3.4.4 Flash

From Figure 8(a) and 8(b), it can be observed that the 2D contour and 3D surface plots, respectively, of flash point demonstrate a consistent increase in flash point with increasing NHAp and NKc concentrations, with a significantly steeper gradient along the NKc axis, establishing nano-kaolin clay as the principal contributor to flash point improvement. The steeper response along the NKc axis is consistent with the ANOVA results, which show that NKc has a larger statistical influence than NHAp, demonstrating that nano-kaolin is principally responsible for improving the binder's thermal behaviour. Although the interaction term (AB) was not statistically significant from Table 4, the convex surface profile and the highest observed flash point (308°C at 1% NHAp and 8% NKc) suggest a cooperative effect between the modifiers that improves thermal stability while decreasing volatility. This shows that NHAp's role is primarily complementary, supporting NKc in increasing the binder's thermal resistance rather than having a substantial interaction effect. The continuous upward trend without a plateau within the studied range indicates sustained improvement across the experimental domain, which translates into improved production safety and thermal ageing resistance, supporting the binary nanomodification approach's effectiveness for high-temperature asphalt applications. The increased flash point implies that greater temperatures are required before the binder produces enough vapour for ignition, enhancing handling safety during asphalt manufacturing and placement. This observation is consistent with the findings of [15], which found that nanoparticles increase the thermal stability and ageing resistance of bituminous binders. Thus, the improved flash point demonstrates that the NHAp-NKc composite successfully boosted the thermal performance of the binder.

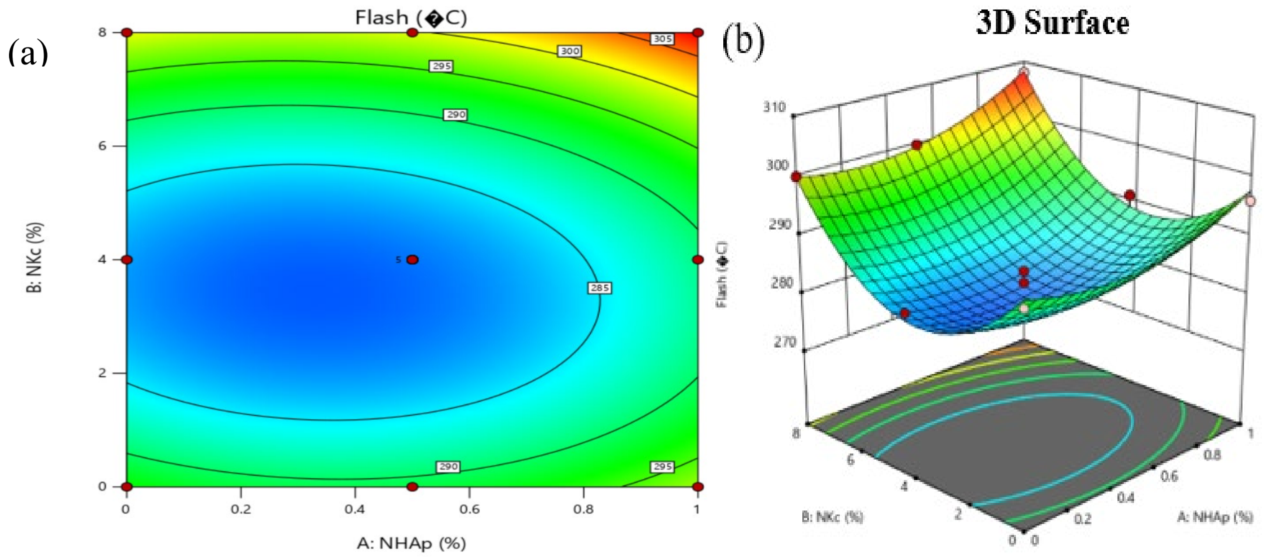

Figure 8: Diagnostic plots for Flash (a)2D contour (b) 3D

3.3.4.5 Fire point

The 3D surface from Figure 9(b) displays a convex, dome-shaped profile with a distinct maximum plateau, while the 2D contour plot from Figure 9(a) displays closed, elliptical contours forming a distinct peak region, confirming a significant interaction effect between NHAp and NKc (AB, p = 0.0107), in contrast to the non-significant interaction observed for flash point. The elliptical contour pattern demonstrates that both modifiers improved the fire point at the same time, indicating a true synergistic interaction between NHAp and NKc. The maximum achievable fire point is limited by the excessive simultaneous addition of both modifiers, most likely because of competing heat processes or particle agglomeration, as seen by a slight saddle behaviour at the highest combined dosages. This implies that increasing the modifier contents over the optimum level provides minimal additional benefit, emphasising the need of optimizing the hybrid composition. The optimal region is found at roughly 0.8% NHAp and 7% NKc, when fire point values are close to 320°C, which is approximately 27°C higher than the control binder. This suggests that NKc is the key contributor to better sustained-combustion resistance, with NHAp playing a secondary, dose-sensitive role. The higher fire point indicates that the improved binder is more resistant to continuous burning, which improves thermal stability at extreme service temperatures. This finding provides compelling evidence for the claim made by [15] that nano-clay improves bituminous binders' ageing resistance and thermal stability.

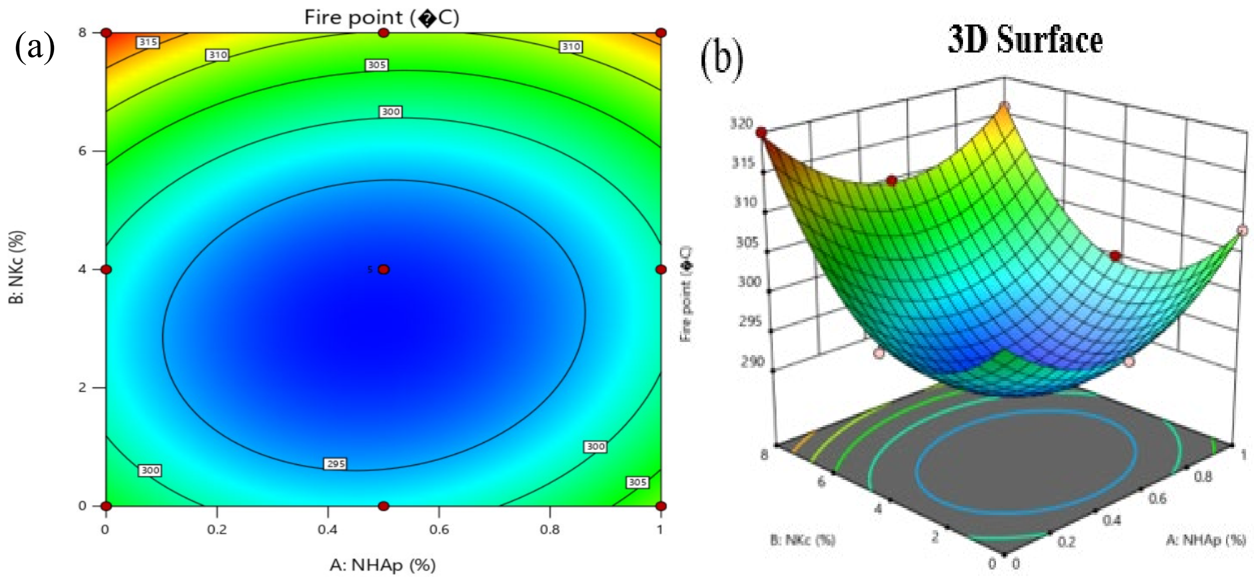

Figure 9: Diagnostic plots for Fire point (a)2D contour (b) 3D

3.3.4.6 Viscosity

From Figure 10 (a), the 2D contour plot shows that viscosity increases more pronouncedly with increasing NKc content, suggesting that NKc has the greatest impact on the rheological behaviour of the binder, which is in line with its really strong impact (p 0.0001). NHAp also adds to the increase, although to a lesser level (p = 0.0002), while the interaction between the two additions shows that their combined effect strengthens the binder structure even more (AB, p = 0.0060). These findings show that both modifiers made a considerable contribution to enhancing binder consistency, with NKc having the greatest influence on viscosity. Previously, a similar increase in viscosity was observed with the addition of polymers 611, 701 and Styrene-Butadiene-Styrene (SBS) by [2] in binder. According to them, adding polymers in bitumen at the rates of 2 %, 2.5 %, 3 %, 3.5 %, and 4 % increased the viscosity values by 2.2, 2.5, 3.2, 3.8, and 4.9 times at 135 °C, respectively, compared to the control. This pattern is clearly illustrated by the 3D surface, which rises toward increasing additive amounts, indicating that the binder becomes progressively stiffer. The upward response surface demonstrates that increasing modifier concentration gradually raises the binder's resistance to flow throughout the experimental range. This behaviour can be explained by the dispersion of nanoparticles within the bitumen, which limits internal molecular movement and hence increases flow resistance. As a result, the modified binder is projected to be more resistant to rutting and permanent deformation under high traffic loads and rising pavement temperatures. The statistical indicators suggest that the model accurately depicts the experimental data, supporting the observed trend's reliability.

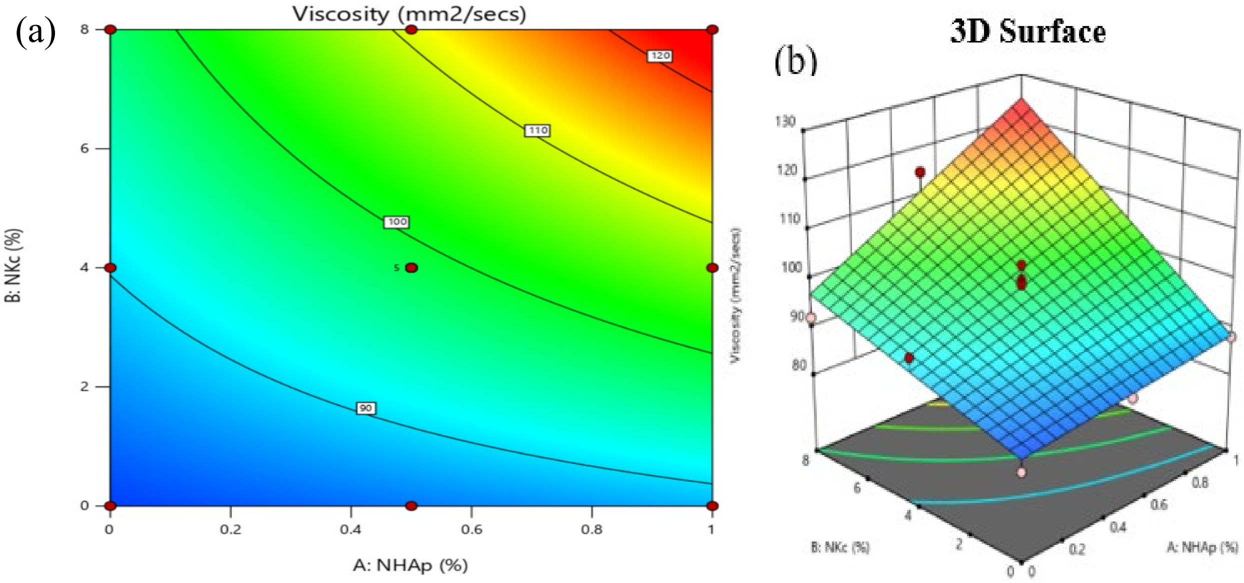

Figure 10: Diagnostic plots for Viscosity (a)2D contour (b) 3D

3.3.5 Fourier Transform Infrared (FTIR) Spectroscopy

Agilent technologies were used to perform FTIR spectroscopy to identify the material based on the functional groups found in its structure. The identification wavelength range was 4000-650 cm-1, with a resolution of 8 cm^{-1} and 16 scans for both the control and optimised asphalt mixtures, as illustrated in Figure 11. The results for both the virgin and optimised asphalt binders show almost the same main functional groups. Strong peaks at 2920 cm^{-1} and 2850 cm^{-1} are seen in both spectra, indicating aliphatic hydrocarbon stretching at the C-H position. Importantly, these peaks are significantly stronger (lower transmittance) for the optimised binder, indicating a more compact interior structure, most likely due to the nanomaterials improving molecular packing. In the optimised sample, a modest broad band between 3400-3600 cm^{-1} associated with O-H stretching appears more obvious, demonstrating hydrogen bonding connected to the surface activity of nano-hydroxyapatite or nano-clay. Both binders have identical peaks in the 1700-1600 cm^{-1} region corresponding to aromatic C-C stretching, but the optimised binder has small shifts and better-defined features, indicating an interaction between bitumen's polar components and the additives, rather than the formation of new compounds. The fingerprint region of the spectra is marked by two significant bands at 1457 cm-1 and 1375 cm^{-1}, representing aliphatic -CH2 and -CH3 bending vibrations, respectively, and a third prominent band at 807 cm^{-1}, representing aromatic C-H bending vibrations. The level of ultraviolet light transmission by the various functional groups in the optimised asphalt binder is noticeably higher than in the control asphalt binder's spectra.

Received: 15/07/2026; Revised: 29/07/2026; Accepted: 09/08/2026; Published: 17/08/2026

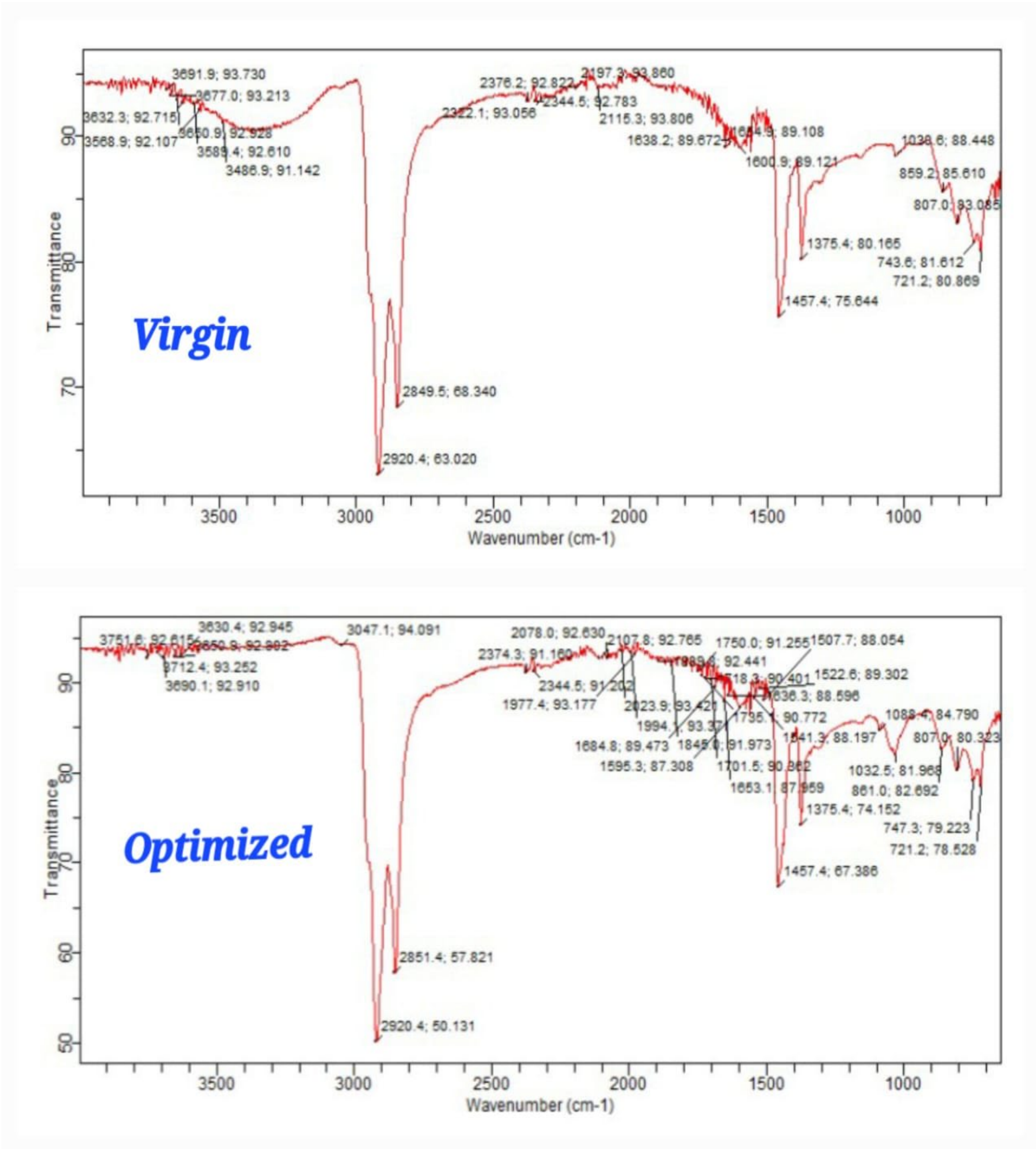

Figure 11: FTIR spectra of Control and Optimised asphalt binder

3.3.6 Optimisation of modified asphalt binder

A numerical multi-objective optimisation method was used to find the best amounts of NHAp and NKc to use to improve the asphalt binder mix. From Table 8, it can be seen that the ductility, flash point, and fire point values were set to maximise. The ranges given by FMWH (2016) were used for penetration, softening point and viscosity. Based on the highest desirability of 59.0%, the RSM Design Expert software came up with the best mix design solution. Figure (12a and b) shows the optimisation ramps and desirability plot for the independent factors and responses of conventional physical properties tests.

Received: 15/07/2026; Revised: 29/07/2026; Accepted: 09/08/2026; Published: 17/08/2026

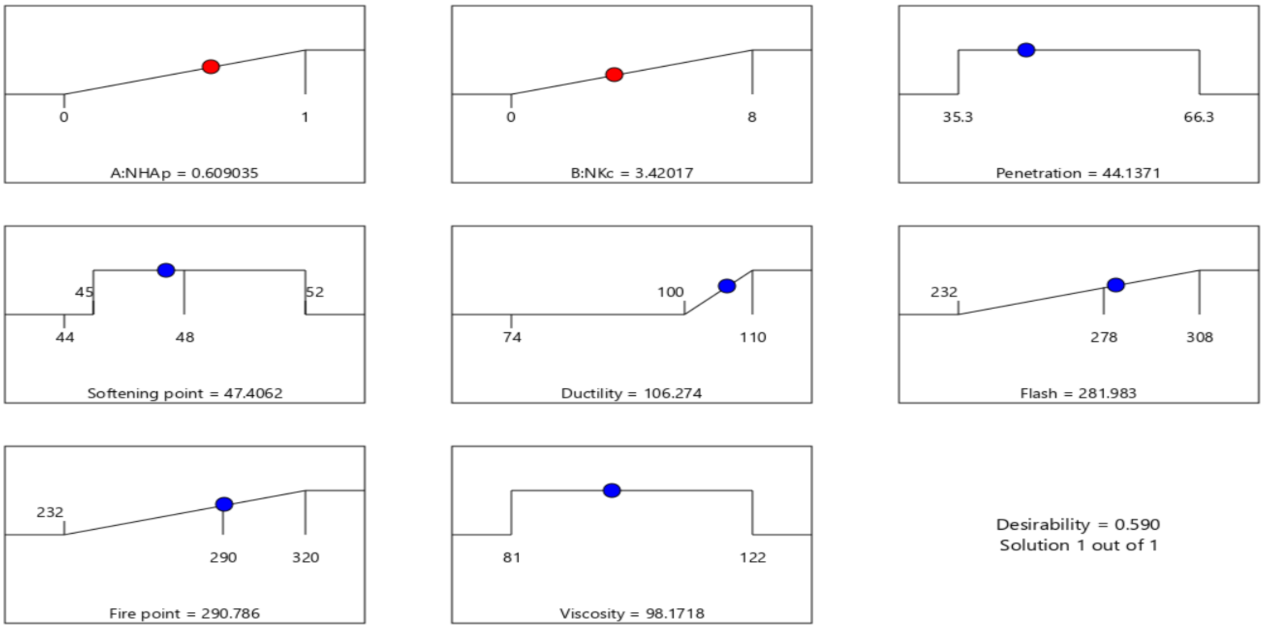

Figure 12 (a): Optimisation ramps

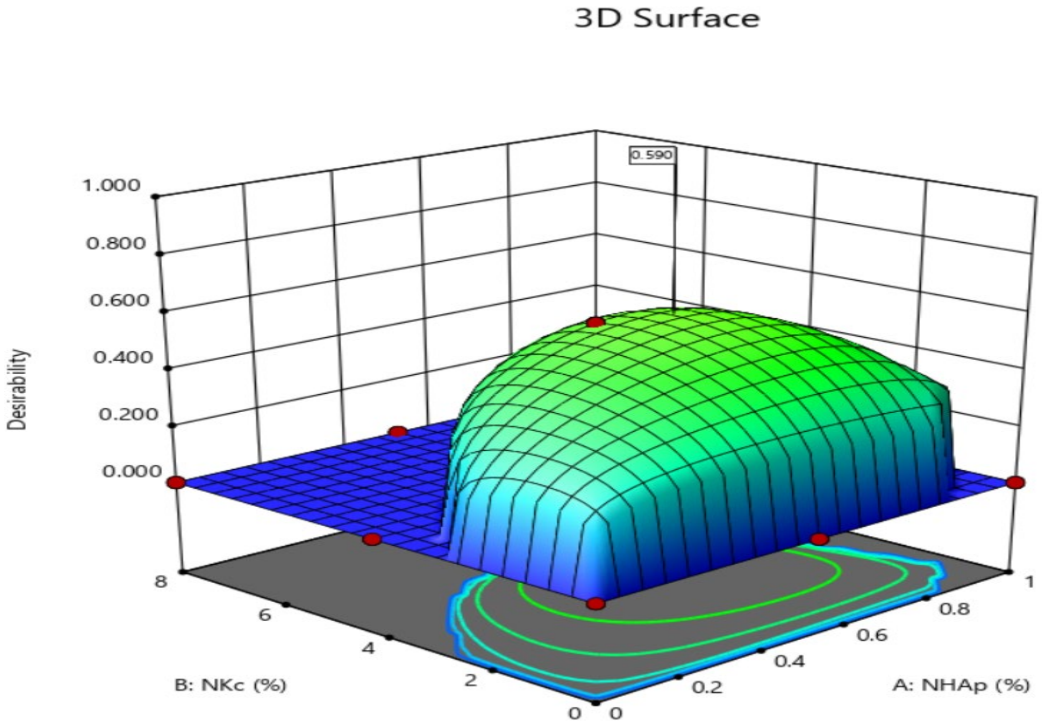

Figure 12 (b): Desirability plot for numerical optimization

Table 8: Numerical optimisation criteria

Parameters	Unit	Desired goal	Lower limit	Upper limit
NHAp	%	Maximize	0	1
NKc	%	Maximize	0	8
Penetration	mm	In range	35.3	70
Softening point	°C	In range	45	52
Ductility	cm	Maximize	100	110
Flash	°C	Maximize	232	308
Fire point	°C	Maximize	232	320
Viscosity	mm^2/secs	In range	81	122

Source: Mamoudou et al. (2026)

Received: 15/07/2026; Revised: 29/07/2026; Accepted: 09/08/2026; Published: 17/08/2026

3.4 Validation of Modified Asphalt binder blend

Additional experiments were carried out to validate the predicted optimum based on the results of the optimal predicted requirements, and a comparison was made with the software's predicted model values. Table 9 presents the results of the validation tests. Equation (8) assesses predictability by calculating the absolute relative percentage error (RPE) between the laboratory and ideally predicted values. The models were highly accurate in predicting the responses, with a percentage error of less than 5% for all responses compared to the laboratory data except for viscosity, which is slightly higher than 5%, demonstrating the model's adequacy.

Table 9 Model validation at optimum conditions

Responses	Unit	Predicted	Experimental	Error (%)
Penetration	mm	44.1403	45.7	3.53
Softening point	°C	47.4071	48	1.25
Ductility	cm	106.277	108	1.62
Flash	°C	281.979	285	1.07
Fire point	°C	290.784	298	2.48
Viscosity	mm^2/secs	98.1718	103.5	5.43

Source: Mamoudou et al. (2026)

$$\textbf{Error}\ (\%) = \frac{\textbf{Experimental}-\textbf{Predicted}}{\textbf{Predicted}} * \mathbf{100} \quad (8)$$

4.0 Conclusion

i. The base bitumen met all ASTM standards, confirming its suitability as control. The DLS analysis revealed successful nano-synthesis, with NHAp particles measuring predominantly 30.28 nm and NKc measuring 27.02 nm. XRD analysis confirmed NHAp's calcium-phosphorus concentration (>80%) for improved adhesion, and NKc's silica-alumina content (>94%) for increased stiffness, demonstrating that both materials had the necessary qualities for efficient bitumen modification.

ii. The combined modification significantly improved binder properties compared to unmodified bitumen. Penetration decreased from 66.3mm to 35.3mm, and viscosity increased from 81s to 122s, indicating superior stiffness and rutting resistance. Thermal safety improved markedly with flash point rising from 292°C to 308°C and fire point from 305°C to 320°C. While ductility decreased with increased NKc concentration. ANOVA revealed that both NHAp and NKc played important functions in modifying the base binder.

iii. The RSM models proved statistically robust ($R^2 > 0.94$, $p < 0.05$) with strong predictive accuracy across all responses. Optimisation identified the ideal blend as 0.61% NHAp and 3.42% NKc with 59% desirability. Validation testing confirmed model reliability with errors between 1.07% and 5.43%, demonstrating RSM as an effective tool for designing modified asphalt binders with predictable performance outcomes.

4.1 Recommendations

Based on the findings of this study, the following recommendations are proposed:

1. The hybrid combination of nano-hydroxyapatite (NHAp) and nano-kaolin clay (NKc) is recommended as a sustainable modifier for asphalt binders, as it significantly improved the conventional binder properties, including penetration, softening point, viscosity, flash point and fire point, while maintaining acceptable ductility.
2. The optimum NHAp–NKc combination identified in this study (0.61% NHAp and 3.42% NKc by weight of binder) is recommended for further evaluation in asphalt mixture design and pavement applications, since it provided the best balance between stiffness, thermal stability and workability.
3. Future studies should evaluate the long-term performance of the optimised NHAp–NKc modified binder through rheological and ageing characterisation, including Dynamic Shear Rheometer (DSR), Bending Beam Rheometer (BBR), Rolling Thin Film Oven Test (RTFOT) and Pressure Ageing Vessel (PAV) tests, to establish its suitability under different climatic and traffic conditions.
4. The mechanical performance of asphalt mixtures prepared with the optimised NHAp–NKc modified binder should be investigated, particularly with respect to rutting, fatigue cracking, moisture susceptibility and low-temperature cracking, to validate the binder-level improvements observed in this study.
5. Further research should examine the microstructural and chemical interactions between NHAp, NKc and bitumen using advanced characterisation techniques, such as SEM, FTIR, XRD and Atomic Force Microscopy (AFM), to better understand the modification mechanisms responsible for the observed improvements.

Received: 15/07/2026; Revised: 29/07/2026; Accepted: 09/08/2026; Published: 17/08/2026

6. A comprehensive life-cycle cost and environmental assessment is recommended to quantify the economic and sustainability benefits of using waste-derived nano-hydroxyapatite in asphalt pavement construction, thereby supporting its practical implementation in sustainable road infrastructure.

4.2 Contribution to Knowledge

This study contributes to knowledge by demonstrating the synergistic effectiveness of waste-derived nano-hydroxyapatite and nano-kaolin clay as hybrid asphalt binder modifiers. It develops statistically validated predictive models for binder performance, identifies an optimum blend of 0.61% NHAp and 3.42% NKc, and proposes a long-term method to produce high-performance asphalt binders through waste valorisation and nanomaterial optimisation.

References

[1] S. Nizamuddin, Y. J. Boom, and F. Giustozzi, "Sustainable polymers from recycled waste plastics and their virgin counterparts as bitumen modifiers: A comprehensive review," *Polymers (Basel).*, vol. 13, no. 19, 2021, doi: 10.3390/polym13193242.

[2] E. Yalcin and A. Demirbag, "Effects of modified binders obtained from different polymers on conventional and rheological properties," *Constr. Build. Mater.*, vol. 357, no. June, p. 129366, 2022, doi: 10.1016/j.conbuildmat.2022.129366.

[3] H. Liu, M. Zhang, Y. Jiao, and L. Fu, "Preparation Parameter Analysis and Optimization of Sustainable Asphalt Binder Modified by Waste Rubber and Diatomite," *Adv. Mater. Sci. Eng.*, vol. 2018, 2018, doi: 10.1155/2018/3063620.

[4] T. W. Johnson, L. Hashemian, S. Patra, and A. Shabani, "Application of Nanoclay Materials in Asphalt Pavements," *2019 Jt. Conf. Exhib. Transp. Assoc. Canada, TAC Intell. Transp. Syst. Canada, ITSC*, pp. 1–16, 2019.

[5] H. J. Aljbouri and A. H. Albayati, "Effect of nanomaterials on the durability of hot mix asphalt," *Transp. Eng.*, vol. 11, no. January, p. 100165, 2023, doi: 10.1016/j.treng.2023.100165.

[6] L. Picado-santos and J. Neves, *applied sciences A Review of Nanomaterials ' E ff ect on Mechanical Performance and Aging of Asphalt Mixtures*. 2019.

[7] A. Mansourian, A. R. Goahri, and F. K. Khosrowshahi, "Performance evaluation of asphalt binder modified with EVA/HDPE/nanoclay based on linear and non-linear viscoelastic behaviors," *Constr. Build. Mater.*, vol. 208, pp. 554–563, 2019, doi: 10.1016/j.conbuildmat.2019.03.065.

[8] S. G. Jahromi and A. Khodaii, "Effects of nanoclay on rheological properties of bitumen binder," *Constr. Build. Mater.*, vol. 23, no. 8, pp. 2894–2904, Aug. 2009, doi: 10.1016/J.CONBUILDMAT.2009.02.027.

[9] D. O. Obada *et al.*, "Fabrication of novel kaolin-reinforced hydroxyapatite scaffolds with robust compressive strengths for bone regeneration," *Appl. Clay Sci.*, vol. 215, no. September, 2021, doi: 10.1016/j.clay.2021.106298.

[10] E. Pepla, L. K. Besherat, G. Palaia, G. Tenore, and G. Migliau, "Nano-hydroxyapatite and its applications in preventive , restorative and regenerative dentistry : Annali di Stomatologia., V (3): 108-114, 2014," pp. 108–114.

[11] M. R. Hasan, M. Sabri, M. Ghazali, and N. F. Mohtar, "PROXIMATE AND MORPHOLOGICAL CHARACTERISTICS OF NANO HYDROXYAPATITE (NANO HAP) EXTRACTED FROM FISH BONE," no. June 2021, 2020, doi: 10.46754/jssm.2020.12.002.

[12] D. O. Obada, E. T. Dauda, J. K. Abifarin, N. D. Bansod, and D. Dodoo-Arhin, "Mechanical measurements of pure and kaolin reinforced hydroxyapatite-derived scaffolds: A comparative study," *Mater. Today Proc.*, vol. 38, pp. 2295–2300, 2020, doi: 10.1016/j.matpr.2020.06.412.

[13] M. Satar *et al.*, "Performance of Kaolin Clay on Hot-mix Asphalt Properties," p. 12002, 2018, doi: 10.1088/1742-6596/1049/1/012002.

[14] H. Paktin, M. Kumar, V. V. Ram, and S. S. Kar, "Laboratory investigation of high-temperature functional characterization of organo-modified nanoclay-enhanced bitumen," *Results Eng.*, vol. 25, no. December 2024, p. 103982, 2025, doi: 10.1016/j.rineng.2025.103982.

[15] M. A. Macías-Silva *et al.*, "Nanomaterials in construction industry: An overview of their properties and contributions in building house," *Case Stud. Chem. Environ. Eng.*, vol. 10, no. June, 2024, doi: 10.1016/j.cscee.2024.100863.

[16] A. Murana and L. Sani, "Partial Replacement of Cement with Bagasse Ash in Hot Mix Asphalt," *Niger. J. Technol.*, vol. 34, no. 4, p. 699, 2015, doi: 10.4314/njt.v34i4.5.

[17] A. Abdel-Raheem *et al.*, "Investigating the Potential of High-Density Polyethylene and Nano Clay Asphalt-Modified Binders to Enhance the Rutting Resistance of Asphalt Mixture," *Sustain.*, vol. 15, no. 18, 2023, doi: 10.3390/su151813992.

[18] H. P. A. C. Mixture, G. S. Moussa, and A. Abdel-raheem, "Effect of Nanoclay Particles on the Performance

of," 2021.
[19] N. Bala, I. Kamaruddin, M. Napiah, and M. H. Sutanto, "Polymer nanocomposite-modified asphalt: characterisation and optimisation using response surface methodology," *Arab. J. Sci. Eng.*, vol. 44, no. 5, pp. 4233–4243, 2019.
[20] N. Bala, M. Napiah, and I. Kamaruddin, "Nanosilica composite asphalt mixtures performance-based design and optimisation using response surface methodology," *Int. J. Pavement Eng.*, vol. 21, no. 1, pp. 29–40, 2020.

Received: 15/07/2026; Revised: 29/07/2026; Accepted: 09/08/2026; Published: 17/08/2026